Parvalbumin is freely mobile in axons, somata and nuclei of cerebellar Purkinje neurones

Hartmut Schmidt,* Oliver Arendt,* Edward B. Brown,† Beat Schwaller‡ and Jens Eilers*

*Carl-Ludwig-Institut für Physiologie, Abteilung Neurophysiologie, Medizinische Fakultät, Universität Leipzig, Leipzig, Germany
†School of Medicine and Dentistry, Department of Biomedical Engineering, University of Rochester, Rochester, New York, USA
‡Abteilung Histologie, Departement Medizin, Universität Fribourg, Fribourg, Switzerland

Abstract

The Ca^{2+}-binding protein (CaBP) parvalbumin (PV) is strongly expressed in cerebellar Purkinje neurones (PNs). It is considered a pure Ca^{2+} buffer, lacking any Ca^{2+} sensor function. Consistent with this notion, no PV ligand was found in dendrites of PNs. Recently, however, we observed for a related CaBP that ligand-targeting differs substantially between dendrites and axons. Thus, here we quantified the diffusion of dye-labelled PV in axons, somata and nuclei of PNs by two-photon fluorescence recovery after photobleaching (FRAP). In all three compartments the fluorescence rapidly returned to baseline, indicating that no large or immobile PV ligand was present. In the axon, FRAP was well described by a one-dimensional diffusion equation and a diffusion coefficient (D) of 12 (IQR 6–20) $\mu m^2/s$. For the soma and nucleus a three-dimensional model yielded similar D values. The diffusional mobility in these compartments was ~3 times smaller than in dendrites. Based on control experiments with fluorescein dextrans, we attributed this reduced mobility of PV to different cytoplasmic properties rather than to specific PV interactions in these compartments. Our findings support the notion that PV functions as a pure Ca^{2+} buffer and will aid simulations of neuronal Ca^{2+} signalling.

Keywords: calcium, diffusion, diffusion equation, fluorescence recovery after photobleaching.

The intracellular free Ca^{2+} concentration ($[Ca^{2+}]_i$) is a key regulator of fundamental cellular processes. Ca^{2+} acts as a second messenger via specialized Ca^{2+}-binding proteins (CaBPs) that show Ca^{2+}-dependent regulation of downstream effectors. Distinct from such Ca^{2+} sensors are pure buffers, which bind Ca^{2+} but lack a Ca^{2+}-dependent interaction with other proteins (Celio *et al*. 1996). In the following we will use 'CaBP' as the generic term for both sensors and buffers.

Owing to its potent action, the spatiotemporal extent of $[Ca^{2+}]_i$ is strictly controlled by endogenous CaBPs and clearance mechanisms. In this process, mobile CaBPs compete with immobile binding sites and pumps for Ca^{2+} binding. They increase the range of Ca^{2+} signals even if they diffuse at a slower rate than free Ca^{2+} ions (for review see Augustine *et al*. 2003). Besides their binding kinetics, the mobility of the individual CaBPs and their action as buffer or sensor are therefore major determinants of cellular Ca^{2+} signalling.

The CaBP parvalbumin (PV) is expressed in large concentrations in distinct subpopulations of neurones, including specific interneurones in many brain regions and cerebellar Purkinje neurones (PNs) (Celio 1990; Baimbridge *et al*. 1992). It belongs to the family of EF-hand CaBPs and was the first member of this family to be discovered (reviewed in Celio *et al*. 1996). The most prominent member of the EF-hand family is calmodulin, which appears to be the primary Ca^{2+} sensor in eukaryotic cells. On the contrary, PV is typically considered to function as a pure Ca^{2+} buffer,

Address correspondence and reprint requests to Hartmut Schmidt, Carl-Ludwig-Institut für Physiologie, Abteilung Neurophysiologie, Liebigstrasse 27, 04103 Leipzig, Germany.
E-mail: hartmut.schmidt@medizin.uni-leipzig.de

Abbreviations used: ACSF, artificial cerebrospinal fluid; $[Ca^{2+}]_i$, intracellular free Ca^{2+} concentration; CaBP, Ca^{2+}-binding protein; CB*, dye-labelled calbindin; 1D, one-dimensional; 3D, three-dimensional; FRAP, fluorescence recovery after photobleaching; FV, focal volume; IF, immobile fraction; Int, intensity; 20k/40k, FD, 20-kDa/40-kDa fluorescein dextran; M_r, apparent molecular weight; PN, Purkinje neurone; PSF, point spread function; PV, parvalbumin; PV*, dye-labelled PV; SDS, sodium dodecyl sulphate.

although to our knowledge the absence of downstream PV targets has only been shown in frog skeletal muscle cells (Maughan and Godt 1999) and in spines and dendrites of rodent PNs (Schmidt *et al*. 2003a). Although it is tempting to generalize the functional classification of PV as a pure buffer based on these observations, we recently found that the related CaBP calbindin-D28k binds to *myo*-inositol-monophosphatase in spiny dendrites of PNs but not in axons (Schmidt *et al*. 2005). Thus, although PV lacks an interaction partner in dendrites (Schmidt *et al*. 2003a), this observation cannot readily be transferred to other structures, not even within the same cell.

Under physiological conditions, the Ca^{2+}-binding kinetic of PV is slow because it has to be preceded by unbinding of Mg^{2+} for which PV also shows significant affinity. Furthermore, its Ca^{2+} dissociation rate is rather slow (Lee *et al*. 2000). As a result of this particular binding characteristic, PV accelerates the initial decay rate of Ca^{2+} transients and introduces a second component to the decay that summates during repetitive stimulation (Lee *et al*. 2000; Schmidt *et al*. 2003b; Collin *et al*. 2005). Although the functional relevance of this peculiar PV action is still obscure in dendritic Ca^{2+} signalling, for presynaptic sites it has been shown that it modulates short-term plasticity and delayed transmitter release (Caillard *et al*. 2000; Collin *et al*. 2005). Furthermore, PV expression in PNs appears to be 10-fold stronger in the axon (≥ 1 mM) than in the perikarion and dendrites (50–100 μM) (Kosaka *et al*. 1993), which might hint towards a predominantly axonal function. In the light of these findings, it was of particular interest to determine the axonal diffusion of PV and to clarify whether or not a binding partner for PV is present in the axon.

One means of quantifying the cytosolic mobility of CaBPs and to concomitantly identify target proteins, i.e. a possible sensor function, is by fluorescence recovery after photobleaching (FRAP; for a review see Reits and Neefjes 2001; Sprague *et al*. 2004). In the present study, we used two-photon FRAP to investigate the mobility of dye-labelled PV (PV*) in the axon and to search for possible axonal binding partners. In addition, we analysed the mobility of PV* in the soma and nucleus of PNs. Our results indicate that PV* freely diffuses in all three compartments and that none of them contains a large (≥ 9 kDa) or immobile interaction partner, indicating that PV is indeed a mere Ca^{2+} buffer and has no additional sensor function in rodent PNs.

Experimental procedures

Slice preparation and solutions

Acute cerebellar brain slices were prepared from 21–24-day-old mice that were decapitated under isoflurane (Curamed, Karlsruhe, Germany) anaesthesia. The vermis was removed and mounted in a chamber filled with cooled (0–2°C) artificial cerebrospinal fluid (ACSF) below). Parasagittal slices 200 μm thick were cut using a vibratome (HR2, Sigmann Elektronik, Hüffenhardt, Germany) and kept in ACSF at 35°C for 45 min before they were transferred to the recording chamber. Experiments were performed at 20–22°C.

The ACSF contained 125 mM NaCl, 2.5 mM KCl, 1.25 mM NaH_2PO_4, 26 mM $NaHCO_3$, 1 mM $MgCl_2$, 2 mM $CaCl_2$ and 20 mM glucose (pH 7.3–7.4 at 20–22°C when gassed with 95% O_2 and 5% CO_2). The pipette solution was composed of 140 mM potassium gluconate, 10 mM NaCl, 3 mM Mg-ATP, 0.3 mM Na-GTP, 10 mM HEPES, 0.1 mM dye-labelled PV or 0.5 mM fluorescein dextran (FD; 10 or 40 kDa) dissolved in purified water (Sigma, St Louis, MO, USA). The pH was adjusted to 7.3 with KOH. All chemicals were from Sigma. Purified rat recombinant PV expressed in *Escherichia coli* was labelled with Alexa-488 (Molecular Probes, Eugene, OR, USA) as described previously (Schmidt *et al*. 2003a). Labelling conditions (pH 9.0) were selected to preferentially label the α-amino group of PV, while ε-amino groups were not labelled significantly. The labelled protein was purified on a size exclusion column (20 × 0.8 cm, gel volume 10 mL) containing Bio-Gel P-6 (medium, fractionation range 1–6 kDa; Bio-Rad, Hercules, CA, USA) to remove the unbound dye. In general, 0.3–1 mL labelling reaction mixture was applied to the column and eluted with buffer [50 mM $(NH_4)HCO_3$, 0.1 mM $CaCl_2$, pH 8.3]. The molecular Alexa/PV ratio was ∼ 0.8.

Dye loading and electrical recordings

PNs were equilibrated with the dye-containing pipette solution for 30 min in the whole-cell patch-clamp configuration. Up to − 300 pA holding current was injected to keep the membrane potential at − 60 to − 65 mV using an Axopatch 200A amplifier (Axon Instruments Inc., Union City, CA, USA), a LIH 1600 AD/DA converter and Patch Master 1.0 software (HEKA, Lamprecht, Germany). The latter components were also used to control a Pockels cell (model 350–50 KD*P; Conoptics, Danbury, CT, USA). Patch pipettes were pulled from borosilicate glass (Hilgenberg) with a PP-830 puller (Narishige) to resistances of 4–6 MΩ. To allow rapid loading of the cells, the series resistance was kept below 25 MΩ for at least 15 min after breaking into the cell.

FRAP recordings and data analysis

As described in detail previously (Schmidt *et al*. 2003a), two-photon FRAP experiments were performed between 30 and 120 min after the whole-cell configuration had been established using a custom-modified Fluoview 300 laser-scanning microscope (Olympus, Hamburg, Germany) equipped with a mode-locked Ti : sapphire laser (Tsunami; Spectra Physics, Darmstadt, Germany) set to a centre wavelength of 765 nm. The laser intensity was modulated with a Pockels cell and focused on to the specimen by a 60 ×/0.9 NA water immersion objective (Olympus). The fluorescence was detected (photomultiplier tube) and sampled with the Fluoview system in the point mode (sampling frequency 250 kHz, 2 or 0.1–0.2 ms binning for cellular or aqueous FRAP recordings respectively). The laser intensity was set to a monitoring value of 4–10 mW (measured at the exit of the objective). After a 0.3-s baseline recording, a bleach pulse (1–6 ms, 35–65 mW) was applied and the recovery of the fluorescence monitored for 1.5 s. After recording the fluorescence signal, the

specimen background, laser intensity and system background were recorded by defocusing, by deflecting scattered laser light towards the photomultiplier tube, and by completely blocking the laser beam, respectively, using the same intensity protocol.

Data analysis was performed with custom written routines in Igor Pro 5.02 (Wavemetrics, Lake Oswego, OR, USA). The fluorescence data were corrected for the specimen background, and the laser intensity data for the system background. The fluorescence was subsequently divided by the square of the laser intensity (Brown *et al*. 1999), and normalized to the baseline fluorescence. Data were only accepted for analysis if the initial bleaching during the baseline period was less than 15%. The first second of the recovery of the axonal fluorescence (F) was fitted with a one-dimensional diffusion equation of the form

$$F(t) = F_i + F_\infty \sum_{n=0}^{\infty} \frac{(-\beta)^n}{n!} \frac{1}{\left(1 + n + \frac{16Dtn}{\omega_r^2}\right)^{1/2}} \qquad [1]$$

where D is the diffusion coefficient, F_∞ is the postbleach fluorescence after recovery, F_i is an offset from the prebleach amplitude ($F_0 = 1$) which would indicate immobilization of PV*, β is the bleach depth parameter (Brown *et al*. 1999) and ω_r is the radial e^{-2} radius of the two-photon excitation volume. Equation 1 was derived by first determining the time evolution of the concentration distribution in one dimension, which itself can be derived from the full three-dimensional (3D) case [equation V in Brown *et al*. (1999)] by taking the limit as ω_r goes to infinity. The fluorescence signal is then determined by convolving this concentration distribution with a Gaussian beam profile. ω_r was determined from the lateral Gaussian profile of the point spread function (PSF) of our system, measured with 100-nm fluorescent microspheres (Molecular Probes) in water and injected into a cerebellar slice. Mean ± SD ω_r in water was 0.57 ± 0.05 μm and that in the tissue was 0.53 ± 0.01 μm ($n = 10$). The percentage of total immobilized PV* (immobile fraction, IF) is $100 \times F_i$/bleach depth. The bleach depth is the amplitude – measured from F_0 – of the signal immediately after the bleach pulse and related but not identical to β (Brown *et al*. 1999).

The first second of the somatic and nuclear recovery were described with the 3D diffusion equation given in Brown *et al*. (1999), with an added offset to explore possible binding of PV* in these compartments:

$$F(t) = F_i + F_\infty \sum_{n=0}^{\infty} \frac{m^{3/2}(-\beta)^n}{n!(m + bn + (bnmt/\tau_D))} \times \frac{1}{(m + bn + (bnmt/R\tau_D))^{1/2}} \qquad [2]$$

with the characteristic radial diffusion time $\tau_D = \omega_r^2/8D$, and the ratio of the beam dimensions $R = \omega_z^2/\omega_r^2$, where ω_z is the axial e^{-2} radius of the two-photon excitation volume (mean ± SD ω_z was 1.8 ± 0.1 μm in water and 1.95 ± 0.12 μm in slices). The parameters m and b represent the number of photons absorbed per molecule in a fluorescence and bleaching event respectively. Ignoring possible higher-order processes, we used $m = b = 2$, i.e. two-photon events. During fitting, the series were truncated after the sixth partial sum. The reliability of all fits was judged by inspection of the residuals (i.e. data – fit).

Results

FRAP principles and axonal mobility of PV*

We used two-photon FRAP to analyse the mobility of Alexa-488-labelled parvalbumin (PV*) in PNs and to search for indications of PV binding partners. PNs were loaded with PV* via a somatic whole-cell patch pipette for at least 30 min before making FRAP recordings. The pipette contained 100 μM PV*, a concentration similar to or smaller than the assumed somatic or axonal concentration of native PV respectively (Kosaka *et al*. 1993). After the 30-min equilibration time, the morphology of the cells (spines, dendrites, soma, nucleus, axon) could be clearly resolved under two-photon excitation, indicating that PV* had free access to all cellular compartments. For FRAP experiments the laser beam was directed to a single point of interest and a brief high-intensity laser pulse was applied to irreversibly bleach the fluorophores within the focal volume (FV). Subsequently, the recovery of the fluorescence, which reflects diffusion of unbleached PV* molecules from neighbouring regions into the FV, was monitored at low laser intensity (Fig. 1).

The size of the FV was determined from the PSF of the microscope, measured with fluorescent microspheres with diameters (100 nm) well below the optical resolution. From the Gaussian profiles of the microsphere signal the radial (ω_r) and axial (ω_z) radii of the two-photon spot at the e^{-2} fluorescence intensity were determined to be 0.53 and 1.95 μm respectively. Thus, the axonal radius (~ 0.5 μm; Fig. 1) is smaller than ω_z and ω_r, and FRAP in the axon can be regarded as 1D diffusion in a pipe. In analogy to the 3D diffusion equation in Brown *et al*. (1999), we derived a 1D diffusion equation for the axon (equation 1 in Experimental Procedures) that quantifies diffusional mobility in terms of the apparent diffusion coefficient (D). This equation well described individual as well as averaged recordings (Figs 1b and c respectively).

In FRAP experiments, binding of PV* to a large or immobile target would result in a steady-state offset from the prebleach level (Luby-Phelps *et al*. 1995; Star *et al*. 2002; Schmidt *et al*. 2005; for a detailed discussion of FRAP time courses see Reits and Neefjes 2001; Sprague *et al*. 2004). In order to reveal such targets, our diffusion equation included an offset as an additional variable. Normalizing this offset to the maximum decrease in the fluorescence induced during bleaching (bleach depth) quantifies the immobile fraction (IF) of PV* (Luby-Phelps *et al*. 1995; Schmidt *et al*. 2003a, 2005). In the example illustrated in Fig. 1(b), the fluorescence fully returned to the prebleaching level (deviation < 1%), indicating that no IF of PV* was present in the axon. Averaging FRAP recordings obtained at different axonal sites significantly increased the signal-to-noise ratio (Fig. 1c) but yielded indistinguishable offsets. On average (54 FRAP recordings, five cells, three

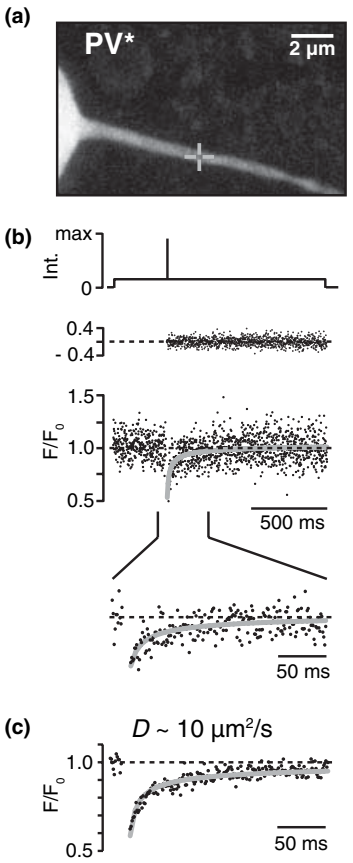

Fig. 1 PV* is freely mobile in axons of PNs. (a) Two-photon image of an axonal segment of a PN filled with 100 µM PV* via a somatic patch pipette (not shown). Part of the soma is visible to the left. The crosshair marks the point of interest from which the FRAP recording illustrated in (b) was taken. (b) Normalized axonal FRAP time course (F/F_0, middle) fitted to a 1D diffusion equation (equation 1 in Experimental Procedures; grey line, $D \sim 12$ µm^2/s). The trace above the recovery curve shows the residuals and the top panel depicts a scheme of the laser intensity protocol (Int.). The lower panel shows the initial 200 ms of the fluorescence recovery on an expanded time scale. Note the rapid and complete baseline return of the fluorescence after the bleach pulse, which indicates the absence of a large or immobile binding partner of PV*. (c) Average of 10 FRAP recordings obtained from the axon in (a) fitted with the 1D diffusion equation (grey line).

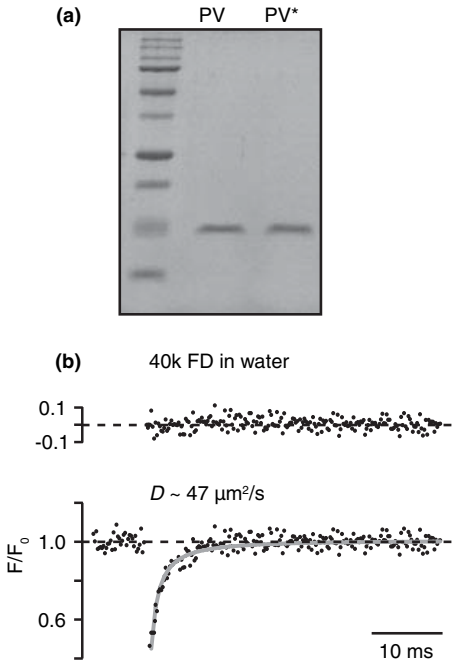

Fig. 2 Quality of PV* and FRAP accuracy. (a) Coomassie Blue-stained SDS–polyacrylamide gel (15%) of 250 µg recombinant PV and PV* (middle and right lanes respectively). The left lane shows molecular weight markers (from bottom to top): 10, 15, 20, 25, 37, 50, 75, 100, 150, and 250 kDa. (b) Average of 50 cuvette FRAP curves of 500 µM 40-kDa (40k) FD in water (lower panel). The grey line represents a fit with a 3D diffusion equation (equation 2 in Experimental Procedures), and the upper panel the residuals.

mice), the mean ± SEM IF was 1.7 ± 1.2%. This value was not significantly different from zero (*t*-test against a hypothetical distribution around zero that had a width and sample size identical to the distribution of the measured IFs). Thus, no significant binding of PV* to a large or immobile partner occurred in the axon.

The presence of small or rapid-kinetic binding partners would be characterized by a reduced diffusional mobility with a smaller *D* value but a full recovery of the fluorescence after bleaching ('retarded' or 'effective diffusion'; Crank 1995; Sprague *et al*. 2004). Such interactions are not readily identified in FRAP recordings but require measurements in different cellular compartments as well as with substances that certainly lack cellular binding partners. Thus, we quantified *D* in the individual axonal recordings and derived a median value of 12 (IQR 6–20) µm^2/s. By averaging recordings from the same axon, performed with identical protocols and showing similar bleach depths (Fig. 1c), we could narrow the error range to a mean ± SEM of 12 ± 2 µm^2/s.

In spiny dendrites of PNs, the *D* of PV* has been reported to be 43 µm^2/s (Schmidt *et al*. 2003a), i.e. a value three to four times larger than the axonal *D* found here. In view of this discrepancy, we controlled the purity and quality of PV* by sodium dodecyl sulphate (SDS)–polyacrylamide gel electrophoresis (Fig. 2a). A single protein band with an apparent molecular weight (M_r) slightly less than 15 kDa (expected $M_r \sim 12$ kDa) was seen in samples with the unlabelled PV and with PV*. As expected the band in the PV* sample migrated slightly more slowly than PV, in line with the small increase in M_r due to the Alexa label. Thus, the reduced axonal mobility of PV does not result from an improper protein.

We further tested whether our experimental approach and the original 3D equation (Brown *et al*. 1999; equation 2 in Experimental Procedures), from which our 1D equation was derived, yields results consistent with published D values. To this end, FRAP measurements were performed in an aqueous solution of 40-kDa FD (Fig. 2b). Four independent samples of 50 averaged recordings each were fitted to equation 2, yielding a mean ± SEM D of 43 ± 5 μm^2/s at 22°C. This estimate is almost identical to the value of 44 ± 5 μm^2/s reported by Arrio-Dupont *et al*. (1996).

Taken together, no technical aspects appeared to account for the observed difference between the axonal and dendritic PV* mobility. Thus, the discrepancy could be indicative of retarded diffusion owing to binding of PV* to a mobile axonal target. On the other hand, differences in cytoplasmic properties (i.e. viscosity and tortuosity) of dendrites and axons could also account for the discrepancy (Crank 1995; Sprague *et al*. 2004). In order to distinguish between these two possibilities we performed axonal FRAP experiments with 10-kDa and 40-kDa FD, for which no cellular interaction partner would be expected. As for PV*, individual and averaged recovery curves were well described by our 1D diffusion equation for both dextrans (Fig. 3). For 10-kDa FD, fluorescence recovery occurred with a median D of 10 (IQR 6–15) μm^2/s (n = 20, four cells, three mice), a value not statistically different from D_{PV}*. The 40-kDa FD, however, recovered significantly more slowly from bleaching than PV* ($p < 0.001$; Mann–Whitney rank sum test). The median D was 5.5 (IQR 3–10) μm^2/s (n = 17, four cells, three mice). In spiny dendrites D values of 32 and 20 μm^2/s have been reported for 10-kDa and 40-kDa FD respectively (Schmidt *et al*. 2003a). These values are again three- to four-fold larger than the present axonal values. This indicates that the reduced axonal mobility of PV* was not due to a specific PV interaction, but instead more likely the result of differences in the cytoplasmic properties of dendrites and axons.

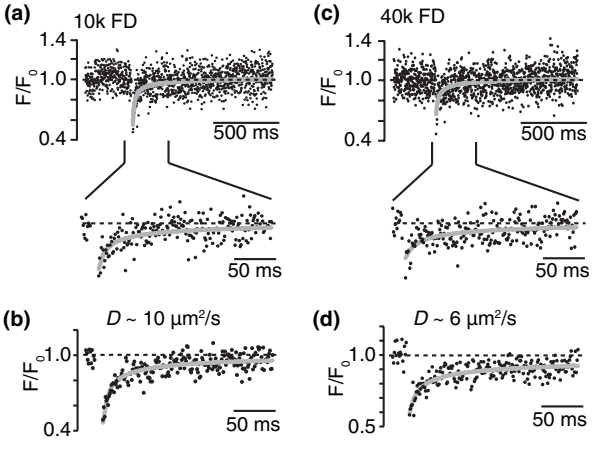

Fig. 3 Axonal diffusion of FDs. (a) Axonal FRAP measured with a 10-kDa (10k) FD and the corresponding fit of the 1D diffusion equation (grey line; $D \sim 8$ μm^2/s). The lower panel shows the first 200 ms of the recovery expanded in time. (b) Fit of the 1D diffusion equation to an average of six recovery curves obtained with 10-kDa FD on the same cell as in (a). (c and d) Same as in (a) and (b) respectively, but with 40-kDa (40k) FD; $D \sim 4$ μm^2/s in (c).

During the experiments, we distinguished between the axon initial segment (~ 20 μm from the soma; Clark *et al*. 2005) and the remainder of the axon. However, no differences were observed in D and IF values between these two axonal segments. Consequently, the data were pooled to represent the axonal mobility. Taken together, the data presented show that no large or immobile PV* binding ligand is present in the axon of PNs and further argue against any specific axonal PV* interactions with small and/or rapid-kinetic partners.

Somatic and nuclear mobility of PV*

We observed that PV* not only labelled the somata of PNs but also reached the nuclei, indicating that PV can readily pass the pores of the nuclear envelope. Because this property is a prerequisite for a transcription factor, such as the recently identified EF-hand CaBP downstream regulatory element antagonist modulator (DREAM) (Carrion *et al*. 1999), in the next set of experiments we analysed FRAP of PV* in the soma and nucleus (Fig. 4). FRAP in these two compartments is governed by 3D diffusion into the FV. Consequently, we used the previously published 3D diffusion equation (Brown *et al*. 1999) to quantify the somatic and nuclear PV* mobility.

We started by exploring possible immobilization of PV* in the soma or nucleus in terms of the IF that was introduced into the fitting function (see equation 2). The mean ± SEM IF in the soma was found to be −1 ± 1% and that in the nucleus was −1.1 ± 3% (Fig. 5a). Thus, within the scatter range, the fluorescence completely recovered to the prebleaching level in both compartments, indicating that there was no significant interaction of PV with a large or immobile partner in either the soma or nucleus.

As in the axon, we next quantified the somatic and nuclear mobility of PV* in terms of the median D. In both compartments, it was found to be 11 μm^2/s [somatic IQR 7–16 μm^2/s (n = 28); nuclear IQR 4–16 μm^2/s (n = 33); five cells each] (Fig. 5b). This value is similar to D in the axon but smaller than that in spiny dendrites (Schmidt *et al*. 2003a). Therefore, we again explored the possibility of retarded diffusion (see above) by performing FRAP experiments with 10- and 40-kDa FD in the soma and the nucleus. Fitting these data with the 3D diffusion equation yielded median D values of 9 (IQR 8–12) and 8 (IQR 7–10) μm^2/s (n = 10, three cells) for somatic and nuclear diffusion of 10-kDa FD respectively (Fig. 5b). For 40-kDa FD, a signifi-

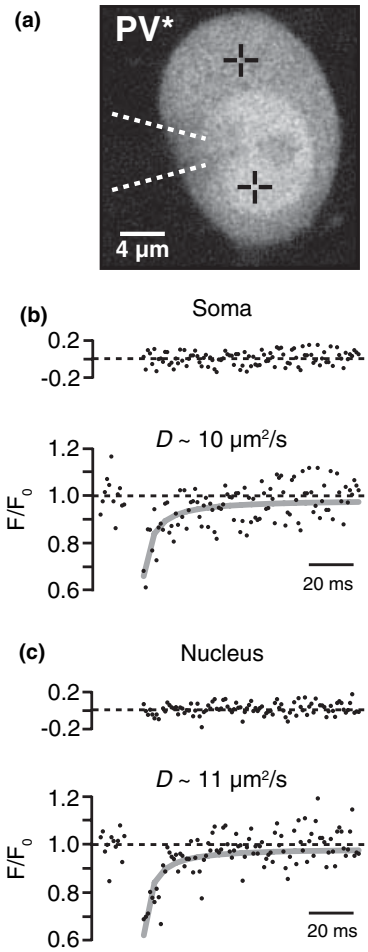

Fig. 4 PV* freely diffuses in somata and nuclei of PNs. (a) PV* labelled the soma and the nucleus. The dashed white lines indicate the position of the patch pipette (not in focus). The cross-hairs mark the points for FRAP recordings shown in (b) and (c). (b) Lower panel: normalized somatic fluorescence recovery and a corresponding 3D diffusion fit (grey line). The upper panel shows the residuals. (c) Same as in (b) but for the nuclear FRAP experiment.

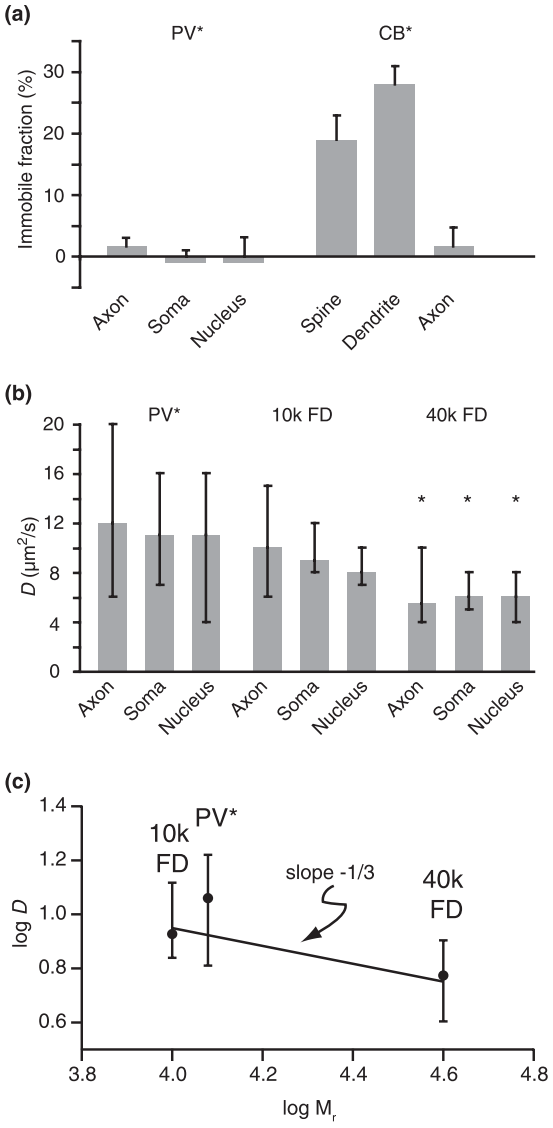

Fig. 5 Summary of FRAP data. (a) The mean + SEM fraction of PV* that remained immobilized on the time scale of the FRAP experiments in axons, somata and nuclei. For comparison, dye-labelled calbindin (CB*) data for spines, dendrites and axons are reproduced from Schmidt *et al.* (2005). (b) Median ± IQR diffusion coefficients (*D*) of PV*, 10-kDa (10k) FD and 40-kDa (40k) FD in axons, somata and nuclei. The asterisks indicate significant differences between the 40-kDa FD data and the PV*/10-kDa FD data (ANOVA, $p \leqslant 0{,}001$). (c) Logarithms of the median *D* values of 10-kDa FD, 40-kDa FD and PV* plotted against the logarithms of their M_r values. The line represents a fit to the FD data with the slope set to − 1/3.

cantly smaller median *D* of 6 µm²/s was found in both compartments [somatic IQR 5–8 µm²/s ($n = 17$); nuclear IQR 4–8 µm²/s ($n = 15$); three cells each; $p \leq 0.001$, Mann–Whitney rank sum test). Thus diffusion was three- to four-fold slower than that in dendrites (see above), providing evidence against specific PV* interactions in the soma and nucleus of PNs.

Relationship between diffusional mobility and molecular weight

The Stokes–Einstein relationship predicts that in aqueous environments the *D* value of molecules much larger than water molecules is proportional to their hydrodynamic radius. Thus, for relatively large molecules, such as dextrans, *D* should be approximately proportional to the inverse cubic root of the M_r (Pusch and Neher 1988; Koch 1999). We previously found that this relationship holds for dextrans in dendrites, but is much steeper for CaBPs (Schmidt *et al.* 2003a, 2005).

We tested for the Stokes–Einstein relationship in axons, somata and nuclei by plotting the logarithms of the obtained

D values of FDs and PV* against the logarithms of the corresponding M_r values (Fig. 5c). For this analysis, the data of the three compartments were pooled. We found a good overlap for the dextran values, with a regression line with the slope set to − 1/3. Similar to the situation in dendrites, a clear (but here non-significant) deviation of PV* from this line was observed. Thus, as in dendrites, the Stokes–Einstein relationships appear to hold approximately when comparing FDs of different M_r in axons, somata and nuclei but presumably not in comparing FDs and proteins. This discrepancy is most likely explained by the tertiary structure of FDs and proteins (Kretsinger and Nockolds 1973; Arrio-Dupont *et al*. 1996).

Given that the Stokes–Einstein relationship holds for FDs and an even steeper dependency might be expected for CaBPs (Schmidt *et al*. 2005), we tried to estimate the smallest size of a PV binding ligand that would be revealed in our FRAP experiments with statistical confidence. To this end, we systematically varied the *D* values obtained for 10-kDa FD until we derived a *D* that was significantly smaller than D_{PV}*. This 'statistically distinct *D*' takes into account the scatter of the data and the sample size. Based on the Stokes–Einstein relationship it was converted to a 'statistically distinct M_r' for a PV binding partner. This conversion yielded an upper limit for an undetected ligand of 9 kDa.

Discussion

Using two-photon FRAP experiments, we quantified diffusion of the endogenous CaBP PV in the axon, soma and nucleus of cerebellar PNs and found no indications for a PV binding ligand in these compartments. Because there was also no evidence in spiny dendrites for binding of PV to intracellular targets (Schmidt *et al*. 2003a) our data substantiate the notion that, at least in PNs, PV functions as a Ca^{2+} buffer and lacks a Ca^{2+} sensor function.

Diffusional exchange between neuronal dendrites and spines is often quantified by exponential fitting of FRAP time courses (Svoboda *et al*. 1996; Majewska *et al*. 2000; Star *et al*. 2002; Schmidt *et al*. 2003a, 2005). In order to provide comparability between different cellular compartments, this approach requires conversion of the time constants (τ) into *D* values. Because τ is related to *D* by the morphology of the structure under investigation, this presupposes a detailed anatomical knowledge. For example, the spino-dendritic τ reflects diffusion *through* a pipe (the spine neck), whereas the axonal τ results from diffusion *within* a pipe. Obviously, τ values cannot be compared directly. Our equation for 1D diffusion offers the advantage that a detailed knowledge of the morphology under investigation is not required, as long as the diameter of the cellular structure is well below the axial and radial extension of the FV. Thus, the present approach can be applied to thin cylindrical structures such as axons and distal dendrites.

The possibility of PV binding to target molecules was explored in two ways: in terms of the IF, which is revealed by an incomplete recovery of fluorescence after bleaching, and by comparing the diffusional mobility of PV* with that of 10- and 40-kDa FD. It has been shown previously that the IF is a convenient measure to identify intracellular targets of dye-labelled proteins if the following criteria are met. First, the target molecule has to be immobile or at least of considerable size and, second, the off rate of the interaction has to be small compared with the diffusional mobility (Luby-Phelps *et al*. 1995; Reits and Neefjes 2001; Star *et al*. 2002; Sprague *et al*. 2004; Schmidt *et al*. 2005). Thus, the observed absence of an IF in all three compartments argues against the presence of a large or immobile PV ligand.

In the axon, the absence of an IF came to some extent as a surprise. Based on quantitative immunogold staining, the PV concentration in axons of rat PNs has been estimated to be $\sim$1 mM and $\sim$100 μM in somata and dendrites (Kosaka *et al*. 1993), suggesting partial immobilization of PV in the axon as a possible adsorption mechanism. How can we reconcile this discrepancy with our FRAP data? First, it could be that PV is incorporated into a stable protein complex, such that our dye-labelled PV could not replace the native PV. However, given that our experiments were performed between 30 and 120 min in the whole-cell configuration, this would require complex stabilities of several hours, which we consider unlikely. Second, in several cases it was observed that CaBP antibody recognition depends on the Ca^{2+}-binding status of the protein (Winsky and Kuznicki 1996; Zimmermann and Schwaller 2002; B. Schwaller and P. Racay, unpublished data). Thus, differences in the metal-binding status of PV in different compartments might yield 'apparent' concentration differences. Finally, the previously reported densities of immunogold particles in axons and somata or dendrites varied by a factor of only 2.5 (Kosaka *et al*. 1993). The subsequent concentration estimate was based on an *in vitro* standard curve that showed a strong non-linearity above PV concentrations of $\sim$100 μM, rendering the concentration estimates between 100 μM and 2 mM rather error prone. Taken together, there is no obvious cause for the discrepancy between the immunohistochemical data and our FRAP data. This topic requires further investigation.

FRAP in the presence of small or rapid-kinetic binding partners is characterized by retarded diffusion with a smaller *D* value but a full fluorescence recovery after bleaching ('effective diffusion'; Crank 1995; Sprague *et al*. 2004). We found that D_{PV}* values in axons, somata and nuclei were three times smaller than those in spiny dendrites of rodent PNs (Schmidt *et al*. 2003a) and in frog myoplasm (Maughan and Godt 1999). This raised the possibility of 'retarded diffusion' of PV* owing to the existence of a small, non-dendritic binding partner. Based on experiments performed with FDs, however, we exclude the existence of PV* interaction sites with $M_r \geq 9$ kDa. Thus, the reduced mobility

may be explained either by systematic errors in our experimental approach or by differences in cytoplasmic properties between dendrites and axons; it is unlikely to reflect specific interactions.

The experimental and theoretical approach taken here has previously been shown to yield *D* values for green fluorescent protein diffusion consistent with the literature (Swaminathan *et al*. 1997; Brown *et al*. 1999). Furthermore, in the present study we demonstrated that the aqueous mobility of 40-kDa FD is also consistent with published values (Arrio-Dupont *et al*. 1996), making it unlikely that our experimental design or mathematical formulae led to systematically reduced *D* values. Thus, we consider differences in the cytoplasmic properties as a more likely cause. These may include the viscosity, tortuosity, and the density of fibres or organelles in the respective cytosolic compartments. For example, microtubules in axons are usually more closely spaced than those in dendrites. Furthermore, although characteristic somatic organelles such as the Golgi apparatus or rough endoplasmic reticulum extend into proximal dendritic structures, they diminish at more distal sites (Fiala and Harris 2005). In the nucleus a high concentration of chromatin (Lafarga *et al*. 1991) could contribute to the reduced mobility of PV*.

To conclude, we have presented evidence that PV lacks specific intracellular targets in cerebellar PNs and so probably functions as a pure Ca^{2+} buffer in these cells. The obtained *D* values provide a foundation for realistic simulations of neuronal Ca^{2+} signalling in the presence of PV.

Acknowledgements

We thank G. Bethge for technical assistance. This work was supported by grants from the Bundesministerium für Forschung und Technologie and the Human Frontier Science Program to JE and the Swiss National Science Foundation (grant 3100A0-100400/1) to BS, and a Whitaker Biomedical Engineering Award (RG-05-0007) and a Department of Defense Breast Cancer Research Program Award (W81XWH-05-1-0396) to EBB.

References

Arrio-Dupont M., Cribier S., Foucault G., Devaux P. F. and d'Albis A. (1996) Diffusion of fluorescently labeled macromolecules in cultured muscle cells. *Biophys. J.* **70**, 2327–2332.

Augustine G. J., Santamaria F. and Tanaka K. (2003) Local calcium signaling in neurons. *Neuron* **40**, 331–346.

Baimbridge K. G., Celio M. R. and Rogers J. H. (1992) Calcium-binding proteins in the nervous system. *Trends Neurosci.* **15**, 303–308.

Brown E. B., Wu E. S., Zipfel W. and Webb W. W. (1999) Measurement of molecular diffusion in solution by multiphoton fluorescence photobleaching recovery. *Biophys. J.* **77**, 2837–2849.

Caillard O., Moreno H., Schwaller B., Llano I., Celio M. R. and Marty A. (2000) Role of the calcium-binding protein parvalbumin in short-term synaptic plasticity. *Proc. Natl Acad. Sci. USA* **97**, 13 372–13 377.

Carrion A. M., Link W. A., Ledo F., Mellstrom B. and Naranjo J. R. (1999) DREAM is a Ca^{2+}-regulated transcriptional repressor. *Nature* **398**, 80–84.

Celio M. R. (1990) Calbindin D-28k and parvalbumin in the rat nervous system. *Neurosci.* **35**, 375–475.

Celio M. R., Pauls T. and Schwaller B., eds. (1996) *Guidebook to the Calcium-Binding Proteins*. Oxford University Press, Oxford.

Clark B. A., Monsivais P., Branco T., London M. and Häusser M. (2005) The site of action potential initiation in cerebellar Purkinje neurons. *Nat. Neurosci.* **8**, 137–139.

Collin T., Chat M., Lucas M. G., Moreno H., Racay P., Schwaller B., Marty A. and Llano I. (2005) Developmental changes in parvalbumin regulate presynaptic Ca^{2+} signaling. *J. Neurosci.* **25**, 96–107.

Crank J. (1995) *The Mathematics of Diffusion*, 2nd edn. Oxford University Press, Oxford.

Fiala J. C. and Harris K. M. (2005) Dendrite Structure, in *Dendrites* (Stuart G., Spruston N. and Häusser M., eds), pp. 1–34. Oxford University Press, Oxford.

Koch C. (1999) *Biophysics of Computation: Information Processing in Single Neurons*. Oxford University Press, Oxford.

Kosaka T., Kosaka K., Nakayama T., Hunziker W. and Heizmann C. W. (1993) Axons and axon terminals of cerebellar Purkinje cells and basket cells have higher levels of parvalbumin immunoreactivity than somata and dendrites: quantitative analysis by immunogold labeling. *Exp. Brain Res.* **93**, 483–491.

Kretsinger R. H. and Nockolds C. E. (1973) Carp muscle calcium-binding protein. II. Structure determination and general description. *J. Biol. Chem.* **248**, 3313–3326.

Lafarga M., Berciano M. T. and Garcia-Segura L. M. (1991) Freeze-fracture organization of chromatin and cytoplasm in neurons and astroglia of rat cerebellar cortex. *J. Neurocytol.* **20**, 533–551.

Lee S.-H., Schwaller B. and Neher E. (2000) Kinetics of Ca^{2+} binding to parvalbumin in bovine chromaffin cells: implications for $[Ca^{2+}]$ transients of neuronal dendrites. *J. Physiol. (Lond.)* **525**, 419–432.

Luby-Phelps K., Hori M., Phelps J. M. and Won D. (1995) Ca^{2+}-regulated dynamic compartmentalization of calmodulin in living smooth muscle cells. *J. Biol. Chem.* **270**, 21 532–21 538.

Majewska A., Brown E., Ross J. and Yuste R. (2000) Mechanisms of calcium decay kinetics in hippocampal spines: role of spine calcium pumps and calcium diffusion through the spine neck in biochemical compartmentalization. *J. Neurosci.* **20**, 1722–1734.

Maughan D. W. and Godt R. E. (1999) Parvalbumin concentration and diffusion coefficient in frog myoplasm. *J. Muscle Res. Cell. Motil.* **20**, 199–209.

Pusch M. and Neher E. (1988) Rates of diffusional exchange between small cells and a measuring patch pipette. *Pflügers Arch.* **411**, 204–211.

Reits E. A. and Neefjes J. J. (2001) From fixed to FRAP: measuring protein mobility and activity in living cells. *Nat. Cell Biol.* **3**, E145–E147.

Schmidt H., Brown E. B., Schwaller B. and Eilers J. (2003a) Diffusional mobility of parvalbumin in spiny dendrites of cerebellar Purkinje neurons quantified by fluorescence recovery after photobleaching. *Biophys. J.* **84**, 2599–2608.

Schmidt H., Stiefel K., Racay P., Schwaller B. and Eilers J. (2003b) Mutational analysis of dendritic Ca^{2+} kinetics in rodent Purkinje cells: role of parvalbumin and calbindin D_{28k}. *J. Physiol. (Lond.)* **551**, 13–32.

Schmidt H., Schwaller B. and Eilers J. (2005) Calbindin D28k targets *myo*-inositol monophosphatase in spines and dendrites of cerebellar Purkinje neurons. *Proc. Natl. Acad. Sci. USA* **102**, 5850–5855.

Sprague B. L., Pego R. L., Stavreva D. A. and McNally J. G. (2004) Analysis of binding reactions by fluorescence recovery after photobleaching. *Biophys. J.* **86**, 3473–3495.

Star E. N., Kwiatkowski D. J. and Murthy V. N. (2002) Rapid turnover of actin in dendritic spines and its regulation by activity. *Nat. Neurosci.* **5**, 239–246.

Svoboda K., Tank D. W. and Denk W. (1996) Direct measurement of coupling between dendritic spines and shafts. *Science* **272**, 716–719.

Swaminathan R., Hoang C. P. and Verkman A. S. (1997) Photobleaching recovery and anisotropy decay of green fluorescent protein GFP-S65T in solution and cells: cytoplasmic viscosity probed by green fluorescent protein translational and rotational diffusion. *Biophys. J.* **72**, 1900–1907.

Winsky L. and Kuznicki J. (1996) Antibody recognition of calcium-binding proteins depends on their calcium-binding status. *J. Neurochem.* **66**, 764–771.

Zimmermann L. and Schwaller B. (2002) Monoclonal antibodies recognizing epitopes of calretinins: dependence on Ca^{2+}-binding status and differences in antigen accessibility in colon cancer cells. *Cell Calcium* **31**, 13–25.